Meas. Sci. Technol. **18** (2007) 3425–3437 doi:10.1088/0957-0233/18/11/024

The response of a silicon diode designed for use as a detector for direct solar radiation

M A Macome[1], J S P Mlatho[2] and M McPherson

Department of Physics and Electronics, North West University (Mafikeng Campus), Private Bag X2046, Mmabatho 2735, South Africa

E-mail: Michael.McPherson@nwu.ac.za

Received 5 June 2007, in final form 2 August 2007
Published 27 September 2007
Online at stacks.iop.org/MST/18/3425

Abstract
A low-cost direct solar radiation detector (DSRD) has been designed, characterized and calibrated. The detector was made of a simple silicon diode and then characterized with respect to spectral response, polar response and environmental stability. It was calibrated by using an Eppley normal incidence pyrheliometer (NIP) mounted on an Eppley power driven sun tracker (ST) whose axis is parallel to the Earth's axis of rotation. The DSRD and the NIP were mounted together on the ST. The results indicate that the DSRD follows the NIP very closely and can therefore be used in its place. The correlation between the DSRD and the NIP data is good with a correlation factor close to unity and a root mean square value close to zero.

Keywords: silicon, detector, solar, radiation, Earth

(Some figures in this article are in colour only in the electronic version)

1. Introduction

An accurate assessment of solar resources is based upon accurately measured data. In particular, data on the spatial distribution of measured solar radiation, especially over a period of time, can be used in models as the basis for many engineering designs and economic decisions. Several authors have clearly given the importance of solar radiation [1–7].

A reliable and sustainable energy supply is very crucial in the context of economic development and may often be used as a measure against poverty. Statistics show that major parts of suburban and rural Africa, and many areas in the world, are located in non-electrified areas [8]. The population in these areas depends on expensive and inconvenient energy sources such as wood, coal, petroleum, paraffin, batteries and candles. These are also the most polluting sources of energy. Solar radiation is a guaranteed and cheap infinite source of energy in any part of the world. This is especially true for rural areas that are situated inside the Sunbelt (40° north to 40° south) [9]. Solar energy does not need a grid connection as compared to some other forms of energy. Solar energy also offers one of the best solutions to the problem of climate change [7]. Solar radiation is the main energy input that determines the physical, chemical and biological dynamics of landscape processes with a direct impact on human living. An understanding of solar radiation in terms of its properties and availability is a logical start to the discussion of its practical application as a source of energy. Any instrument that can be used to measure solar radiation cheaply is of paramount importance. The data gathered on the availability of solar radiation at a particular site can be used to develop and analyse the performance of solar energy systems, in the studies of heat balances in biological and building sciences and in meteorology.

Solar radiation is an electromagnetic wave, the spectrum of which extends from a wavelength of 10^4 to 10^{-12} m [10]. The work presented in this paper focuses specifically on the solar radiation spectrum (SRS) which extends from a wavelength of ∼300 to ∼3000 nm. The SRS is divided into three main regions: the ultraviolet (UV) region of wavelength between ∼300 and ∼380 nm; the visible region of wavelength

[1] Now at Departamento de Física, Universidade Eduardo Mondlane, Mozambique.
[2] On study leave at North West University from University of Malawi, Malawi.

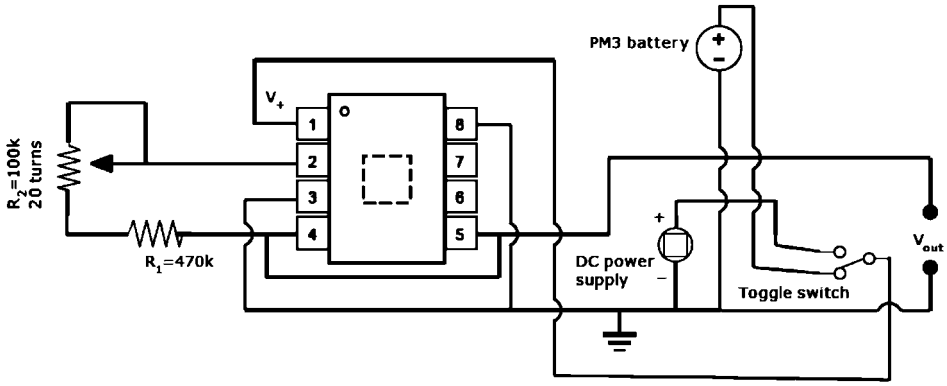

Figure 1. A schematic diagram of the DSRD circuit. After [14].

between ∼380 and ∼780 nm; and the infrared region (IR) which comprises radiation of wavelength greater than 780 nm [11]. A large amount of UV radiation is absorbed by atmospheric particulates before it reaches the Earth's surface. The atmosphere is almost completely transparent to solar radiation in the visible region [12]. Infrared radiation is emitted by all objects that are at temperatures below ∼700 K [10]. The atmosphere absorbs about 20% of the radiation in the IR region.

Direct solar radiation is measured by using direct solar radiation detectors (DSRDs). These detectors are of four types: calorimetric, thermomechanical, thermoelectric and photoelectric [13]. In our work, a DSRD was developed for gathering solar radiation data cheaply and on a real time basis. It was also designed as a user-friendly detector. The DSRD detects radiation by using the quantum detection principle which is based on the direct conversion of solar radiation into an electrical signal. The DSRD is made up of an integrated circuit (IC) and an external circuit (EC), both of which are housed in a black, rectangular and rigid plastic box. Holes for collimation of the solar beam, for the power supply lead and for feeding the electrical signal to a data logger have been drilled into the box. The IC is an OPT101 monolithic combination of a photodiode and an amplifier. The noise performance of the IC depends on the bandwidth in which the amplifier operates, the feedback resistance, the feedback capacitance and the capacitance of the photodiode. The advantage of a monolithic combination is the high possibility of elimination of leakage current errors, the elimination of noise pick-up and gain peaking due to stray capacitance [14]. The time constant of the IC is $RC = 0.71\ \mu$s, which is actually the time in which the IC responds to changes in the measured effect.

The photodiode constitutes the sensing element of the DSRD and has an active area of ∼5.22 mm^2. It is operated in the photoconductive mode, a mode in which it converts the solar radiation falling onto it into an electrical current which is proportional to the amount of solar radiation absorbed. In general, photodiodes respond strongly to the radiation at near-infrared, and this makes thermal noise in such diodes an effect to be strongly taken into account. The amplifier operates as an integrating amplifier and is an inverting operational amplifier. It is connected onto the IC such that the current flowing from the photodiode is converted into a voltage signal which is the output. Thus, the DSRD signal can be read directly by a data logger.

The EC consists of a variable resistor, a battery and a toggle switch. The variable resistor is introduced to adjust the amplification of the signal and also to vary the time constant. The switch allows either the battery or the power supply to be used to bias the detector. A schematic diagram of the DSRD circuit is shown in figure 1. The photodiode is the dashed square in the middle of the IC, R_1 is a resistor for the protection of the photodiode and R_2 is a variable resistor which allows for adjustment of the sensitivity of the detector.

Optical filters are often used to correct the spectral response of semiconductor detectors mainly because they can attenuate or block out certain wavelengths of radiation. They can also enhance the spectral sensitivity of a detector and hence can be used to produce an overall desired detector response [15]. The overall responsivity of a detector is equal to the product of the responsivity of the sensor and the transmission of the filter. Because of this, an ideal filter transmission curve can be obtained if a desired overall sensitivity is given and the responsivity of the detector is known.

Two groups of filters were used in this work and these are distinguished by their construction and the principle of operation. The first group is the interference filter, which is based on a harmonic interference between waves to provide very narrow pass bands. These filters are capable of bandwidths less than 10 nm. An interference filter consists of thin metallic layer films spaced half the desired wavelength apart by a dielectric spacer. The second group of filters is the absorptive filters, and these are based on the absorption of a particular bandwidth. This type of filter consists of glass that has been doped with a certain amount of dye that absorbs particular colours only.

This paper presents details of a silicon diode that has been used as a detector for direct solar radiation. The detector has been characterized and found to be working fairly well in comparison to an industry NIP. It is envisaged that the detector can be deployed *en masse* for the measurement of solar radiation as a replacement of the expensive NIP. The data gathered can be used in the design of solar energy storage systems.

2. Experimental details

The detector designed by our group was characterized with respect to spectral response, to polar response and to

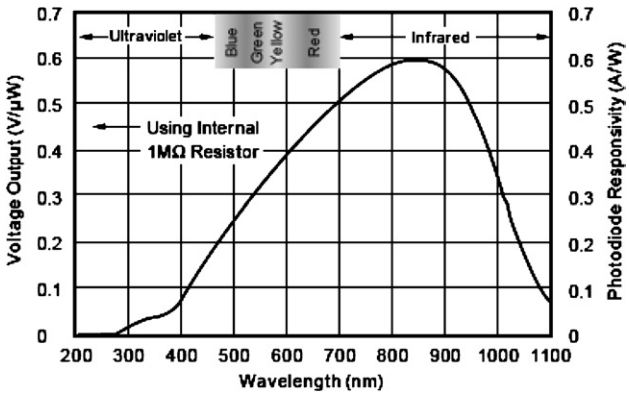

Figure 2. A spectral response of the OPT101 sensor which shows a peak at 850 nm indicating that the detector is more sensitive at this wavelength. After [14].

environmental stability. Below, we discuss the individual aspects of the three experiments.

2.1. The spectral response

The main experiment in this work was the one carried out with respect to the spectral response of the two detectors, DSRD1 and DSRD2. The spectral response (also known as spectral sensitivity) of a detector is the response of the detector with respect to monochromatic light as a function of wavelength. Two particular filters were chosen for the use on the detectors both for the case of a clear day and that of a turbid day. The experiments involved measurements of direct solar radiation using the two detectors for three different situations; with no filter, with a BG39 filter attached and with a KG filter attached.

The DSRD1 is designed to detect solar radiation in the wavelength range between 320 nm and 1100 nm. The characteristic spectral response of the OPT101 sensor shown in figure 2 indicates that the responsivity of the detector is more pronounced in the IR region, with a peak at 850 nm. This means that the detector will indicate a high output when IR radiation is predominant and this occurs when the sun sets. Another contributing factor to the increased output is the significant emission of IR radiation by the Earth and any objects on its surface during the time when the sun sets. This enhances the predominance of IR radiation in the sky and hence increases the readings of the detector.

The BG39 filter is a bandpass Schott filter that allows transmission of radiation only in the range between ∼320 nm and ∼700 nm with a peak at about 500 nm. The thickness of the filter is 1.00 mm and the reflection factor is 0.91. The overall spectral response of the detector representing a combination of the spectral responsivity of the sensor and the Schott glass filter BG39 is shown in figure 3. The figure suggests that the DSRD1 coupled to the BG39 filter will detect direct solar radiation in the wavelength range of ∼350 nm to ∼700 nm. In other words, the overall responsivity of the detector combined with the BG39 filter will be given by the area under the combined responsivity curve. Thus, the DSRD1 in the situation of figure 3 will be less sensitive to solar radiation in the IR region and therefore good for the study for a number of reasons. First, the most important part of the solar radiation spectrum for DRSDs is in the visible region. This is because a major portion of the energy that reaches the Earth's surface is situated in this region. The second reason is that radiation detected in the IR region is small compared to the radiation detected in the visible region. The third reason is that a major part of solar radiation in the IR region is strongly absorbed by water vapour and carbon dioxide in the atmosphere.

The KG filter is a broadband Schott optical glass filter which transmits radiation between the wavelength ranges of ∼400 nm and ∼800 nm. This filter is almost uniformly

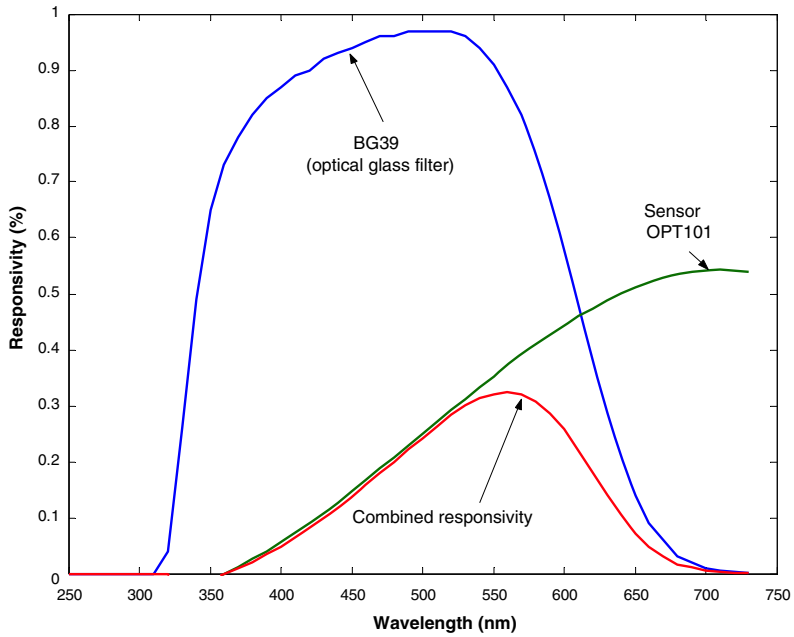

Figure 3. The overall spectral response of the OPT101 sensor and the optical glass filter BG39. The combined responsivity is shifted to a wavelength of ∼550 nm.

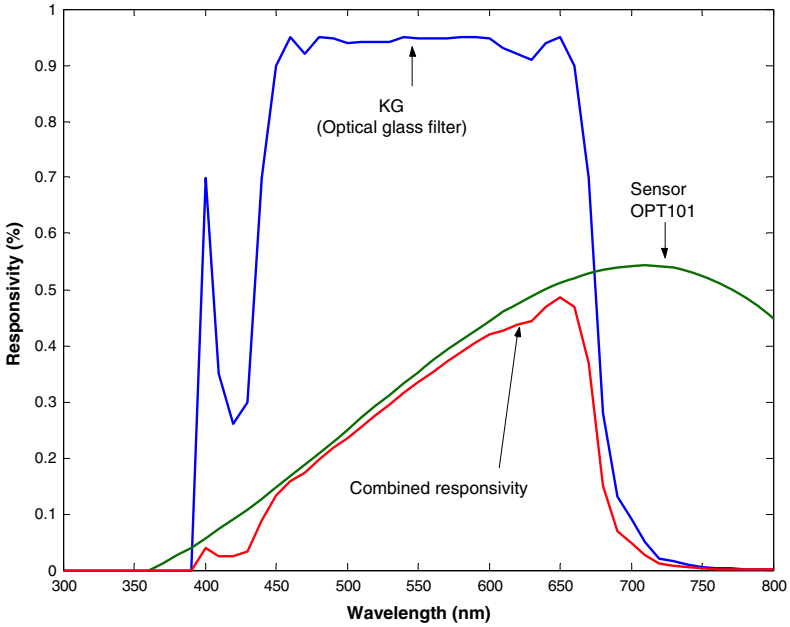

Figure 4. The overall responsivity of a combination of the OPT101 sensor and the optical glass filter KG. The figure indicates a resultant peak responsivity at ∼650 nm.

transparent in the visible region of the SRS but is opaque to the UV and IR radiations. It should therefore be ideal for correction of the spectral response of the DSRD1. A combination of the spectral responsivity of the DSRD1 and the KG filter is shown in figure 4 and it indicates a combined peak responsivity at a wavelength of about 650 nm.

A comparison of figures 3 and 4 shows that a combination of the OPT101 sensor and the BG39 filter produces a responsivity area that is smaller than a combination of the OPT101 sensor and the KG filter. This would seem to imply that the best combination of filter and detector is achieved by the use of the OPT101 sensor and the KG filter. We present results that confirm this assertion.

2.2. The polar response

Polar response is the response of a detector with respect to the angle of incidence of the solar beam. The polar response of the DSRD1 is very important for an assessment of the collimation process. The solar beam is collimated in order to restrict the detection of different and unwanted wavelengths. The collimating hole is 10 mm long and it is of a diameter of 1 mm. The dimensions offer a full angle field of view of about 5.2°, which is an angular aperture from which the detecting surface sees the sun.

For DSRD1, the full angle field of view was chosen by taking into account the fact that the detector was needed to provide a signal from which the flow rate of a heat exchange fluid of a solar thermal energy storage (TES) system could be controlled online. It was also required to determine the saturation value of the detector for dimensions that give a full angle field of view larger than 5.2°. When direct solar radiation was measured without any consideration of the variation of atmospheric conditions, the full angle field of view was found to vary from ∼8° to ∼15°. In the design of solar TES systems, it is ideal to have a full angle field of view ranging between 5° and 6° [16].

In general, an aperture that has a full angle field of view below 4° is not practical for general meteorological purposes. On the other hand, an aperture with a full angle field of view greater than 8° enables an instrument to measure, in addition to direct solar radiation, radiation from the aureole. Under ordinary conditions, counts ranging between 1.5 and 7.0 per cent of the direct solar radiation are possible [17].

2.3. The environmental stability

The test for environmental stability was intended to measure the ability of the detector to withstand changes in ambient temperature, in precipitation, in humidity and in dust content.

The housing of the DSRD1 is black and made of plastic, factors that are significant contributors to the amount of heat absorbed. The absorbed heat should lead to an increase in temperature within the housing and the surroundings of the detector particularly the detecting device which is a simple p-i-n diode. The rise in temperature causes an increase in the measured current [18] in such p-i-n diodes. A temperature sensor was incorporated in the housing of the DSRD2 to investigate the effect of temperature changes on the measured current. The black housing, used in the DSRD1, was replaced with a white housing to reduce possibilities of heat absorption in the DSRD2. It is possible that the effects of heat absorption may only be observed over a long-term period, so that the replacement of the black housing with a white one was assumed as a long-term preventive measure.

The housing of the DSRD1 was not very well sealed and this could have caused damage to the detector by allowing accumulation of moisture and dust onto the detecting surface. Further, unwanted radiation may be detected through these unsealed points, thereby distorting detector readings. A

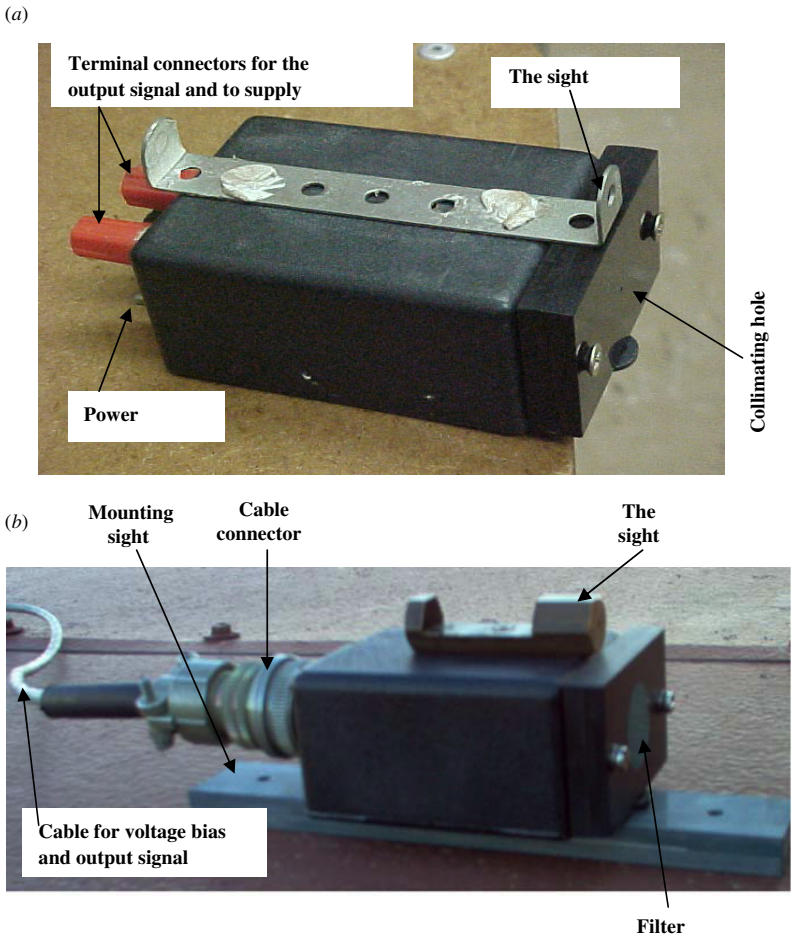

Figure 5. A photograph of the DSRD1 (*a*) and the DSRD2 (*b*). The DSRD2 incorporates various improvements carried out on the DSRD1.

properly sealed housing of the DSRD2 was expected to prevent negative performance of the detector and to provide long-term durability.

Another improvement on the DSRD1 was to use an insulated terminal to connect the cables that feed the signal to the data logger and the voltage to the detector. The DSRD was built such that either a battery or an external power supply could be used. A toggle switch was incorporated to switch on either the battery power supply or the external power supply. The connectors and the toggle switch were, however, not waterproof and not at all suited for corrosive environments. In the case of the DSRD2, a sealed connector was used which holds six pins through which signals could be transmitted. This connector is water and dust proof.

A black perspex block 10 mm thick and with a collimating hole was placed in front of the box. The block was placed such that the solar beam could be focused through the hole to the detecting surface. The filter was placed in such a way that besides filtering solar radiation it could also act to block moisture and dust from accumulating in the collimating hole. In these ways, the interior of the housing could be assumed to be completely sealed from the outside and also assumed to be at a temperature tolerable to the detecting surface. Figure 5 is a photograph of the DSRD1 (*a*) and the DSRD2 (*b*) showing various improvements carried out on the DSRD1.

3. Results and discussion

We present results of the spectral response in the first case, of the polar response in the second case and finally of the environmental stability in the third case.

3.1. The spectral response

The results presented here were taken on a clear sky day for the three different cases when no filter was incorporated, when the KG filter was attached and when the BG39 filter was attached. Similar data were also taken for a turbid day but we shall not present these here as the data obtained on a clear day makes our point adequately. We compare the results of the DSRDs to those of the NIP, the reference instrument.

3.1.1. The DSRD1. An important aspect of the experiment is the way that the DSRD1 readings track the variation of solar radiation as given by the reference instrument. The results are shown in figure 6. The red curve is a plot of direct solar radiation expressed in volts and measured using the DSRD1. The blue curve is a plot of direct solar radiation also in volts, measured using the reference instrument. The scaling on the vertical axes is different due to the difference in magnitude between the readings of the DSRD1 and the NIP, the DSRD1 readings being about six times larger than

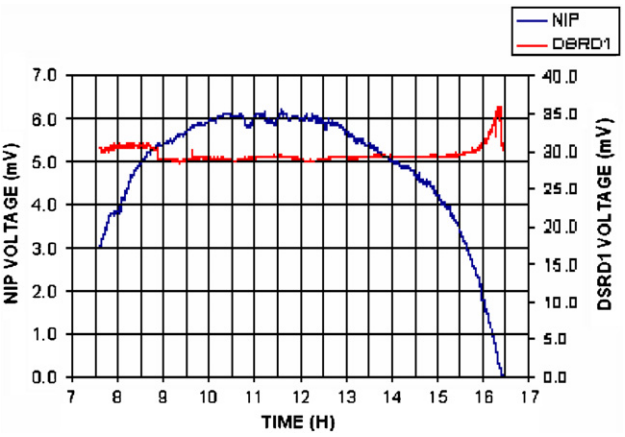

Figure 6. A plot of direct solar radiation measured in volts using the DSRD1 with no filter and the NIP. The voltage applied to the DSRD1 was supplied from a 9 V battery.

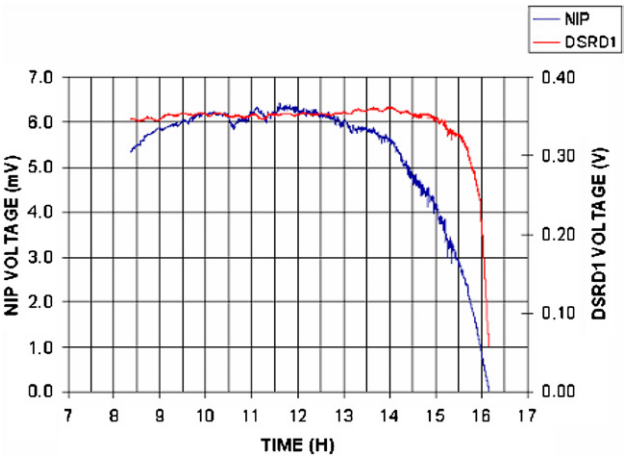

Figure 7. A plot of direct solar radiation measured in volts using the DSRD1 (coupled to the KG filter) and the NIP. A 9 V battery was used as the voltage supply to the DSRD1. Note that the right-hand side scale is given in V.

those of the NIP. The same axis system is used to enable a comparison in terms of how the measurements taken with the DSRD1 track the characteristic variations of solar radiation according to measurements obtained from the NIP. The graph of the reference instrument shows an increase in solar radiation intensity from sunrise to about 11:30 after which it starts to decrease until sunset at about 16:30. For a clear sky day, this is the expected behaviour of the variation in direct solar radiation intensity measured at sea level, taking into account the attenuation of solar radiation. In contrast, the graph of direct solar radiation measured using the DSRD1 shows no significant variations in intensity between about 07:30 and 15:30, after which it shows an increase towards sunset. This is a clear indication of the malfunction of the DSRD1 for measuring direct solar radiation simply because it should read zero at sunset. Because there is more IR radiation towards sunset, it means that the DSRD1 is more sensitive to this type of radiation. The first filter used is thus aimed at filtering out this radiation.

Our first attempt to correct the spectral response of the DSRD1 was by the use of a cut-off glass filter, KG. The results of the performance of the DSRD1 coupled to the KG filter are indicated in figure 7. The figure shows no significant difference in the readings given by the DSRD1 except that towards sunset the profile shows a decrease in the direct solar radiation measured. This is contrary to the results plotted in figure 6. Another observation is that the magnitude of the signal from the DSRD1 has decreased dramatically by two orders of magnitude. The effect of IR radiation as indicated in figure 6 is not present here, which suggests that the filter is working to prevent IR radiation from the detecting element. Thus, the incorporation of the KG filter somewhat improves the spectral response of the DSRD1.

In figure 8, we present a plot of solar radiation measured with the DSRD1 (coupled to the BG39 filter) and the NIP. The plot indicates that the spectral response of the detector has been modified although it is still not tracking the variations of the direct solar radiation properly as shown by the results from the reference instrument. At 09:00 and at 09:30 the solar radiation measured by the DSRD1 increased abruptly before levelling off after which it decreased rapidly. These results disagree with

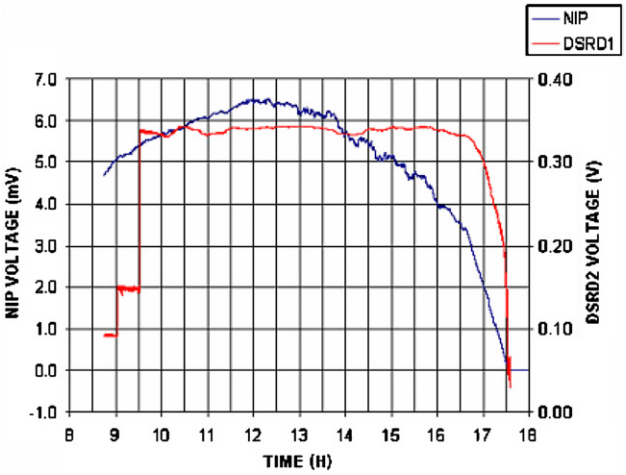

Figure 8. A plot of direct solar radiation measured in volts using the DSRD1 (coupled to the BG39 filter) and the NIP. The voltage to the DSRD1 was supplied from a 9 V battery. Note that the right-hand side scale is given in V.

those given by the reference instrument. However, the results indicate that the filter is working to block out any incident IR radiation. In this case too, the incorporation of the BG39 filter has somewhat improved the spectral response of the DSRD1.

The spectral response of the DSRD1 with no filter, with the KG filter and with the BG39 filter suggests that the detector sensitivity is more pronounced in relation to IR radiation since this type of radiation is predominant at sunset. Another observation is that the DSRD1 responds equally during the day, especially over the period when solar radiation should reach a peak value. This suggests that this poor correlation could be due to some alteration of the original characteristics of the detector, which could have been caused by exposure to moisture and dust. This means that the detecting element of the DSRD1 has been damaged. It is for this reason that the DSRD2 was built using a sensing element with the same characteristics as those of the one in the DSRD1.

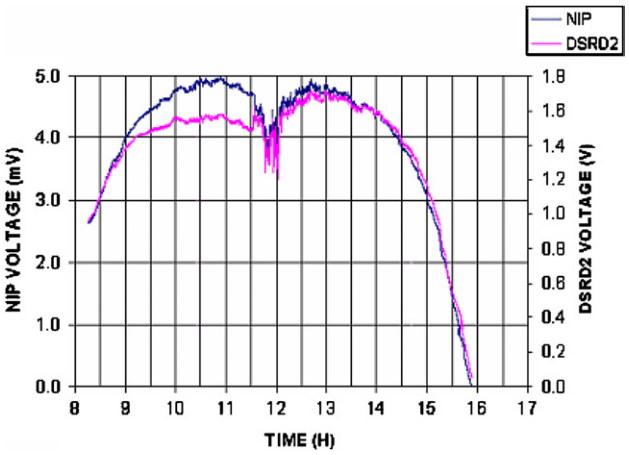

Figure 9. A graph of direct solar radiation measured in volts using the DSRD2 and the NIP. The voltage to the DSRD2 was supplied from a 30 V power supply unit.

3.1.2. The DSRD2. The DSRD2 was mounted together with the NIP on the sun tracker for a comparison of their responses. A plot of direct solar radiation measured in volts using the DSRD2 and the NIP is shown in figure 9.

The pink curve is a plot of solar radiation measured using the DSRD2 and the blue curve is a plot of solar radiation measured using the NIP. The data indicate that the DSRD2 with no filter tracks variations in direct solar radiation in a similar manner as the reference instrument. Since the sensing element is the same in both the DSRD1 and the DSRD2, this means that the optical properties of the sensing element on the DSRD1 must have been altered. This may have been caused by moisture and dust that could have accumulated in the housing and onto the surface of the sensor. This could have happened because the housing of the DSRD1 is not properly sealed. The DSRD2 graph does not, however, exactly follow the NIP graph especially just before midday when the NIP reads higher than the DSRD2. The fact that the readings of the DSRD2 between ∼08:45 and ∼12:15 are lower than those of the NIP suggests that the response of the sensor in the DSRD2 is dependent on the wavelength of solar radiation. This means that the DSRD2 responds better to radiation at the near-infrared region, which occurs in the period from sunrise until ∼09:00 and from around 15:00 when the sun moves towards sunset. However, the traces indicate that even if the correlation is not good, the detecting device in the DSRD2 can be used to measure direct solar radiation with a reliable accuracy.

Figure 10 shows a plot of the correlation between readings taken with the DSRD2 and those taken with the NIP. Also shown in red is a fit to the data and this can be used to correct the small imperfections in the readings of the DSRD2 that are observed. The plot shows a significant deviation of the calibration curve in relation to the plot of correlation from 1.5 mV of the NIP voltage.

The calibration curve displayed is a polynomial function of the eighth order given by

$$P = P_1x^8 + P_2x^7 + P_3x^6 + P_4x^5 + P_5x^4 + P_6x^3 + P_7x^2 + P_8x + P_9, \quad (1)$$

where $P_1, P_2, P_3, \ldots, P_9$ are the polynomial coefficients whose values are given in table 1 and x represents the data points. In table 1, the sum square error (SSE) is a measure of the total deviation of data points from the fitting, R^2 is the root square that indicates how successful the fit is for calibration of the DSRD2 with respect to the reference instrument and RMSE is the root-mean-square error which shows how far the evaluated points are from the reference. A good fit will have $R^2 \sim 1$ and RMSE ~ 0.

The value of R^2 is not close to unity and this means that the readings given by the DSRD2 without incorporating any filter are not close to those given by the reference instrument. This

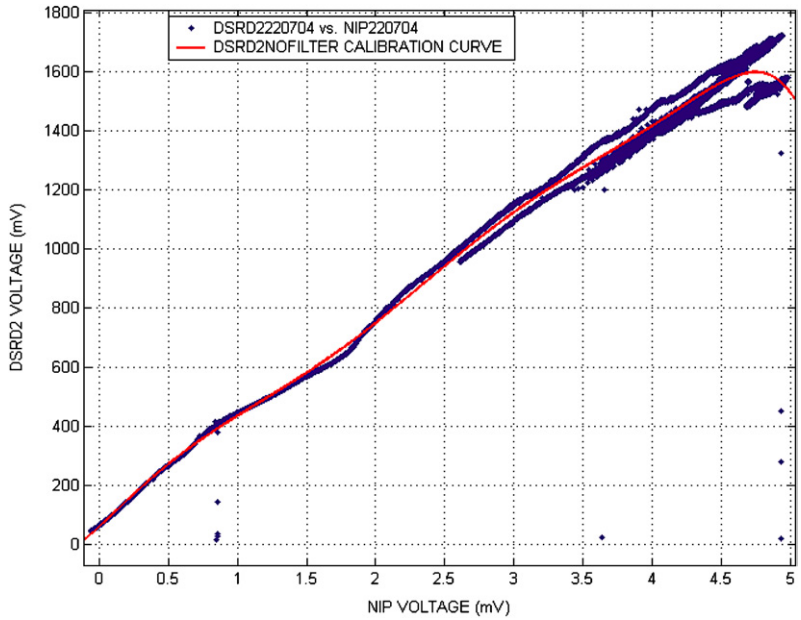

Figure 10. A correlation graph between the DSRD2 (with no filter) and the NIP data. The red curve represents the calibration factor which must be taken into account to correct the readings of the DSRD2 in order that they agree with those of the NIP.

Table 1. A summary of the polynomial coefficients of the calibration curve and errors introduced by measuring direct solar radiation with no filter attached to the DSRD2.

	Polynomial coefficient								
Data set	P_1	P_2	P_3	P_4	P_5	P_6	P_7	P_8	P_9
No filter	−0.0976	0.5482	6.586	−70.55	240.6	−323.4	87.07	435.4	58.25
	The goodness of fit								
	SSE			R^2				RMSE	
	72.33			0.976 38				0.514	

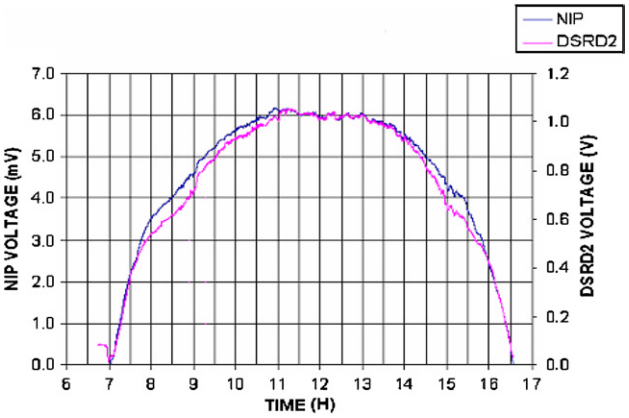

Figure 11. A plot of direct solar radiation measured in volts using the DSRD2 and the NIP. The DSRD2 incorporates the KG filter. Note that the left scale is given in V.

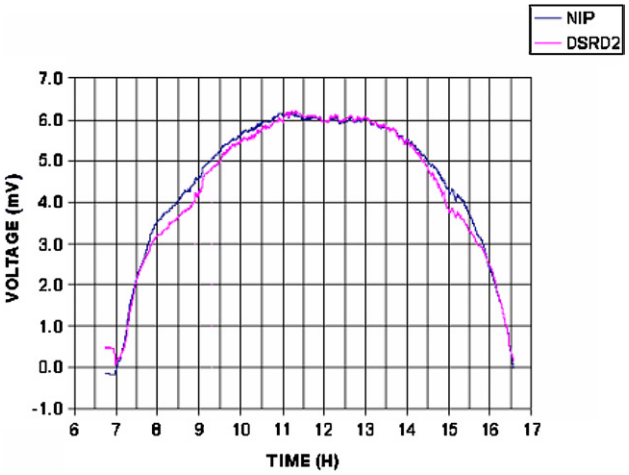

Figure 12. A plot of the direct solar radiation measured in volts using the DSRD2 (and the KG filter) and the NIP. The DSRD2 data have been corrected to the NIP data by a factor of 171.43.

means that the use of the DSRD2 with no filter attached does not provide a better characterization of direct solar radiation that nearly mimics the reference instrument. The value of the RMSE is closer to one than to zero and this means that the DSRD2 does not trace the reference instrument closely, and the deviations of the DSRD2 in relation to the reference instrument cannot be neglected.

Presented in figure 11 is a plot of direct solar radiation measured with the DSRD2 and the NIP. In this case, the DSRD2 has been fitted with the KG filter. The results show that when the DSRD2 is coupled to the KG filter, it tracks the variations in the amount of solar radiation that reach the Earth's surface very well. The differences observed in the morning and in the afternoon between the two data sets are very small as shown by the area between the curves. In either case, however, the DSRD2 reads lower than the reference instrument. These results show a noticeable improvement to the data of figure 9, the case with no filter, especially just before noon.

In order to compare the magnitude of the readings obtained from the two instruments, the measurements obtained with the DSRD2 were corrected to those obtained with the NIP as determined from figure 11. The correction factor is 171.43 (which divides the DSRD2 data) and the result is shown in figure 12. The difference between the readings is low and this indicates that the DSRD2 reads closer to the reference instrument. A comparison of the graphs in figure 12 indicates that the DSRD2 reads lower in the period that extends from 07:45 to 11:00 and also between 14:15 and 16:00. The reason for this difference is that the combined spectral response of the sensing element and the KG filter (according to figure 4) varies with respect to the wavelength of solar radiation. Nevertheless, the use of the KG filter has improved the spectral response of the DSRD2 considerably.

Figure 13 is a plot of the correlation between data obtained using the DSRD2 incorporating the KG filter and data obtained using the NIP. The plot also shows the calibration curve. The figure reveals that the DSRD2, when fitted with the KG filter, tracks the reference instrument fairly well. The figure also shows a good curve fit for calibration of the DSRD2 since the calibration curve follows the correlation curve very closely. There is better agreement in this case than there was in figure 9, the case with no filter. This calibration curve is also a polynomial function of eighth order as evaluated by equation (1), with coefficients given in table 2.

The value of R^2 is nearly equal to unity and this means that the readings given by the DSRD2 incorporating the KG filter are nearly equal to those given by the reference instrument. This means that the combination of the DSRD2 and the KG filter provides a better characterization of direct solar radiation which nearly mimics the reference instrument. The value of the RMSE is nearly equal to zero and this means that any deviations in relation to the reference instrument can be considered as negligible.

Presented in figure 14 are the measurements obtained from the DSRD2 and the NIP. In this case, the DSRD2 has been fitted with the BG39 filter. This is our second attempt to correct the spectral response of the DSRD1.

As can be seen from the figure, minor variations in the amount of solar radiation detected are recorded and these are caused randomly by atmospheric conditions. On a clear sky

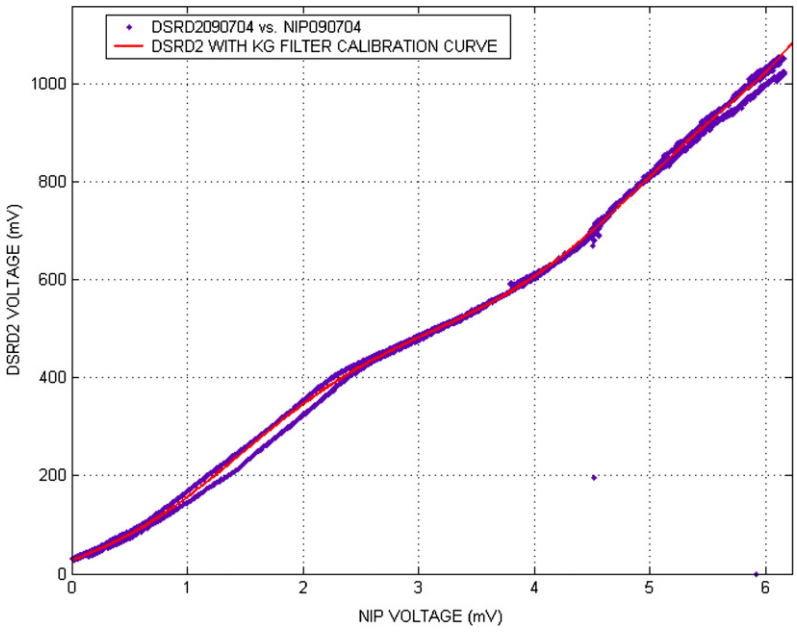

Figure 13. A correlation graph between the DSRD2 (and the KG filter) and the NIP data. The red curve represents the calibration factor which must be taken into account to correct the readings of the DSRD2 in order that they agree with those of the NIP.

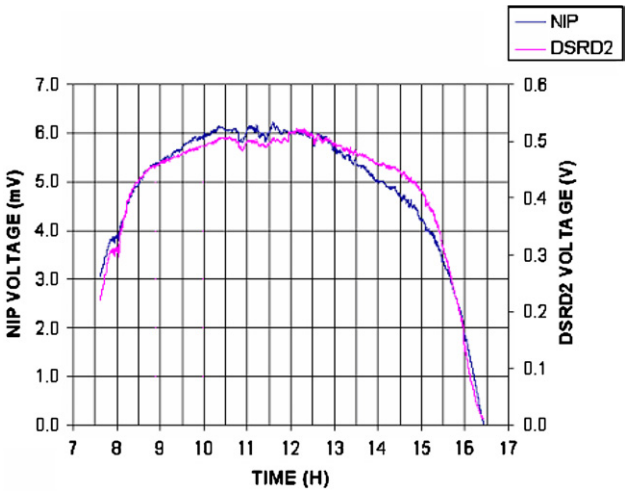

Figure 14. A plot of direct solar radiation measured in volts using the DSRD2 and the NIP. The DSRD2 is fitted with the BG39 filter and the voltage is supplied from the 30 V power supply unit.

day like the case shown in the figure, the amount of solar radiation recorded by the DSRD2 and the NIP increases as the sun rises with a peak at noon. The DSRD2 voltage is about two orders of magnitude higher than the NIP voltage. In general, the graph of figure 14 indicates that the DSRD2, when fitted with the BG39 filter, produces a signal that follows closely the variations in the amount of solar radiation as measured by the NIP. It even records the occurrence of any spontaneous interference. As seen in the previous sections, the magnitude of the signal obtained with the DSRD2 is much higher than that obtained with the reference instrument.

In order to compare the trend and the magnitude, the data obtained from the DSRD2 are corrected to the NIP data by dividing by a factor of 85.71. This result is shown in figure 15. The figure shows that there is generally a good agreement between the DSRD2 and the reference instrument except at two regions starting around 09:30 and 13:30. In the former case (09.30) the DSRD2 reads lower than the reference instrument, while in the latter case (13.30) it reads higher. The former case shows that the DSRD2 fitted with the BG39 filter is less sensitive to direct solar radiation during a period in which the predominant radiation is of a wavelength of $\sim$0.45 μm. This is a period towards the time of maximum solar irradiance when the sun is at solar noon (the closest position in relation to the detector). In the latter case, the DSRD2 has higher sensitivity in the afternoon, a period leading towards maximum temperature when the Earth is beginning to irradiate more of the absorbed radiation.

A plot of the correlation curve between the data obtained with the DSRD2 incorporating the BG39 filter and the data obtained with the NIP is given in figure 16 together with

Table 2. A summary of the polynomial coefficients of the calibration curve and errors introduced by measuring direct solar radiation with the DSRD2 incorporating the KG filter.

	Polynomial coefficient								
Data set	P_1	P_2	P_3	P_4	P_5	P_6	P_7	P_8	P_9
KG	0.013	−0.185	0.060	9.762	−53.81	97.31	−23.81	100.1	26.84
	The goodness of fit								
	SSE			R^2			RMSE		
	0.4112			0.998 78			0.0976		

Table 3. A summary of the polynomial coefficients of the calibration curve and errors introduced by measuring direct solar radiation with the DSRD2 incorporating the BG39 filter.

	Polynomial coefficient								
Data set	P_1	P_2	P_3	P_4	P_5	P_6	P_7	P_8	P_9
BG39	0.011	2.844	−30.44	170.4	−530.9	900.7	−735.8	282.7	−10.9
	The goodness of fit								
	SSE			R^2				RMSE	
	2.228			0.983 44				0.1454	

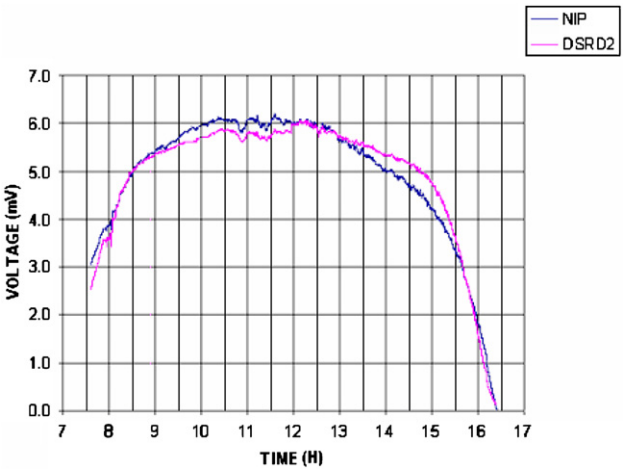

Figure 15. A plot of direct solar radiation measured in volts using the DSRD2 (and the BG39 filter) and the NIP. The DSRD2 data have been corrected to the NIP data by a factor of 85.71.

the fitting curve for calibration of the DSRD2. The graph reveals discrepancies between the correlation curve and the fitting curve. In other words, the fitting curve does not follow the correlation curve. This suggests that a combination of the DSRD2 and the BG39 filter is not good for measuring direct solar radiation since it has a poor agreement with the reference instrument. The second blue line appearing at higher NIP voltages can be explained in a similar manner as in figure 13.

Table 4. A summary of the correlation values between the readings of the DSRD2 and the NIP for the three situations with no filter, with the KG filter and with the BG39 filter.

DSRD2	SSE	R^2	RMSE
With no filter	72.33	0.976 38	0.5139
With the KG filter	0.4112	0.998 78	0.0976
With the BG39 filter	2.228	0.983 44	0.1454

The R^2 value shown in table 3 is closer to unity as compared to that in table 1. In addition, the RMSE value in table 3 is less than the RMSE in table 1. The values of R^2 and RMSE in table 3 imply that the BG39 filter does improve the performance of the DSRD2.

Table 4 summarizes the R^2 and RMSE values for the three situations of no filter, the KG filter and the BG39 filter. Comparing R^2 and RMSE values from all the three cases shows that the performance of the DSRD2 is better when it has a filter coupled to it. The filter that best suits the desired overall

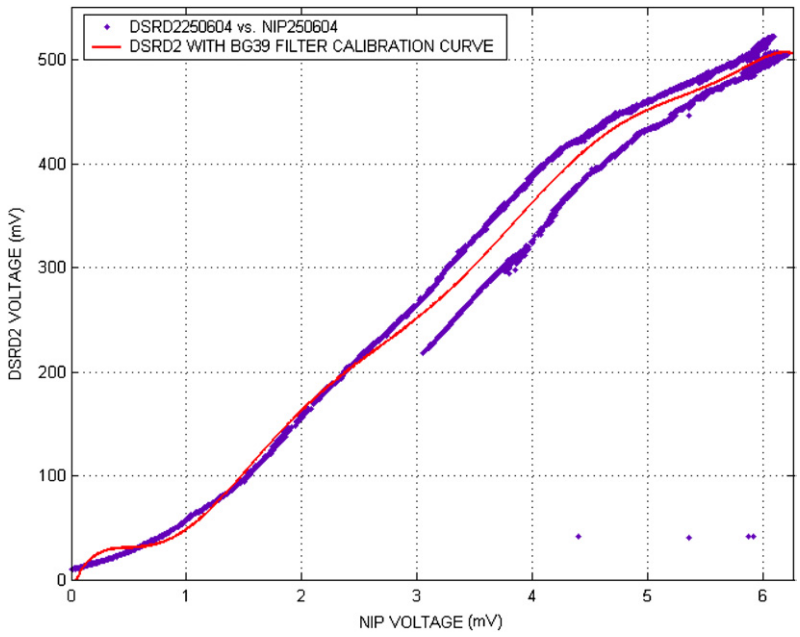

Figure 16. A correlation graph between the DSRD2 (and the BG39 filter) and the NIP data. The red curve represents the calibration factor which must be taken into account when correcting the readings of the DSRD2 in order that they are of the same magnitude as those from the reference instrument.

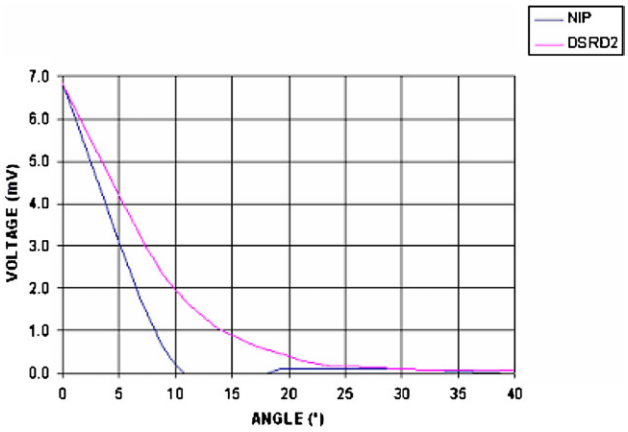

Figure 17. A graph of direct solar radiation measured in volts using the DSRD2 and the NIP for different angles of incidence of the solar beam. The DSRD2 incorporates no filter.

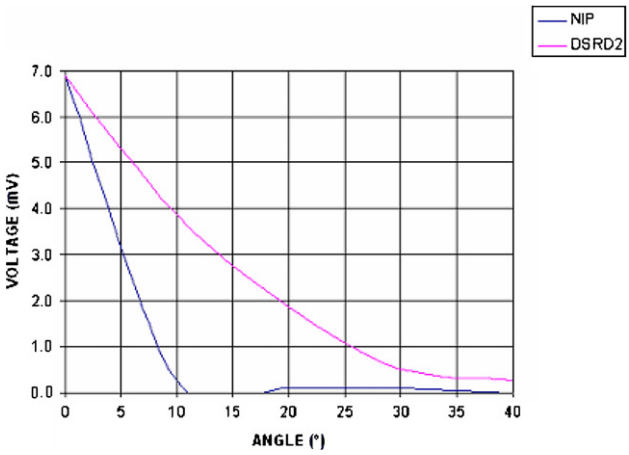

Figure 18. A graph of direct solar radiation measured in volts using the DSRD2 and the NIP for different angles of incidence of solar beam. The DSRD2 incorporates the KG filter.

spectral response for the detector is the KG filter. This is because with this filter the SSE and RMSE values are close to zero while the R^2 values are close to unity, which is the ideal condition for a good curve fit.

3.2. Polar response

The results presented here were taken on a clear sky day for the three different cases of no filter incorporated, the KG filter incorporated and the BG39 filter attached to the DSRD2. All measurements were carried out using the manual sun tracker, thus the accuracy of the measurements is assumed to provide an approximate idea of the goodness of the collimating hole of the DSRD2.

3.2.1. The DSRD2 with no filter attached. Figure 17 is a plot of the direct solar radiation measured in volts using the DSRD2 and the NIP against the full angle field of view. The plot shows how the amount of energy measured varies with respect to the angle of incidence of the solar beam. The curve in pink is the response of the DSRD2 and the curve in blue is the NIP response. The values of the direct solar radiation measured in volts using the DSRD2 were divided by a factor of 174.52 in order to correct the magnitude of the readings to the readings of the reference instrument. This allowed that the graphs generated by the two instruments could be plotted on a single graph for comparison.

The plot indicates a higher response (of nearly 7 mV) by both instruments when the angle of incidence of the solar beam is equal to zero. This occurs when the solar beam strikes the surface of the sensing element at a perpendicular angle. This highlights the importance of the alignment of the detector in relation to the direction of the solar beam. Fairly good readings are obtained up to about 10°, after which both instruments read very poorly. Beyond 25°, the instruments read virtually zero volts.

A comparison of the graph of the DSRD2 and that of the NIP indicates that the DSRD2 still detects radiation beyond 10° while the NIP detects no radiation at all. This is most probably because the collimating hole of the DSRD2 is cylindrically shaped whereas the one of the NIP is conical. The cylindrical shape of the hole in the DSRD2 allows the detection of radiation that has undergone multiple reflections. However, the characteristic responses are similar in that the sensitivity of the detectors to the incident solar beam decreases with the increase of the angle of incidence of the solar beam.

3.2.2. The DSRD2 with the KG filter attached. The results of the DSRD2 (incorporating the KG filter) and the NIP are shown in figure 18. The graphs indicate similar behaviour of the instruments, that is a reduction in sensitivity occurs with an increase of the angle of incidence of the solar beam, a maximum detectable being 7 mV at 0°. However, the DSRD2 detects higher than the NIP for the angles of incidence greater than zero. It also detects beyond 10°, while the NIP does not. As already stated, this may probably be because the collimating hole of the DSRD2 is cylindrical whereas that of the NIP is conical.

A comparison of the polar response of the DSRD2 given in figure 17 for the situation with no filter and that given in figure 18 for the situation with the KG filter shows that the DSRD2 trace is moved further away from the NIP trace. Thus, the DSRD2 with no filter reads lower (∼2 mV at 10°) than the DSRD2 with the KG filter (∼4 mV at 10°). This suggests that the KG filter enhances the polar response of the detector and this is due to the refractive properties of the filter.

3.2.3. The DSRD2 with the BG39 filter attached. Figure 19 is a plot of the results obtained with the DSRD2 (incorporating the BG39 filter) and the NIP. The DSRD2 has a polar response in which a reduction in sensitivity occurs with an increase in the angle of incidence of the solar beam. However, one aspect noticeable is that the trace indicates that the DSRD2 tends to over read in the interval ranging from ∼4° to ∼19°. It detects beyond 10°, however, while the NIP does not. This suggests that the refractive properties of the BG39 filter enhance the polar response of the DSRD2.

A comparison of the results of the polar response of the DSRD2 given in figure 18 for the situation of the KG filter and that given in figure 19 for the situation of the BG39 filter highlights the fact that a better angular response is obtained

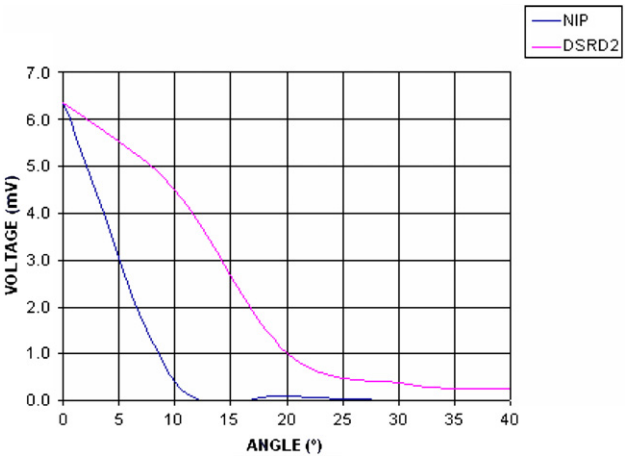

Figure 19. A graph of direct solar radiation measured in volts using the DSRD2 and the NIP for different angles of incidence of solar beam. Here, the DSRD2 incorporates the BG39 filter.

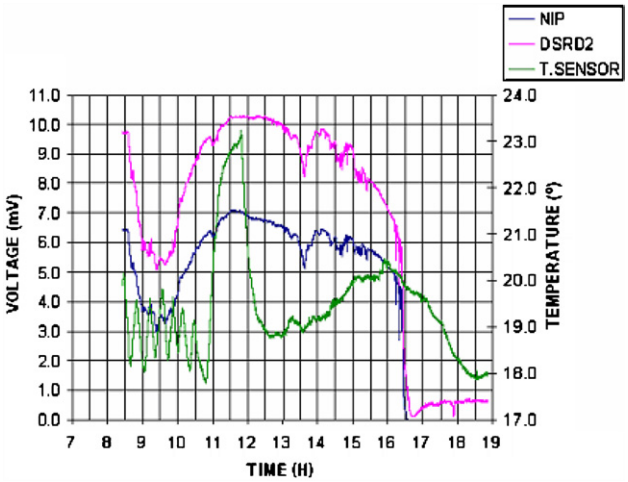

Figure 20. A plot of direct solar radiation measured in volts using the DSRD2 (fitted with the KG filter) and the NIP. A plot of the variations in temperature inside the housing of the DSRD2 is also presented.

with the KG filter. It has been found in section 3.1 that the KG filter improved the spectral response of the DSRD2. It is thus safe to insist that the KG filter is a better filter for our case.

3.3. Environmental stability

In the test for environmental stability, the temperature inside the housing of the DSRD2 was measured using a sensor. This was in order to determine the effect of temperature changes to the output of the DSRD2. The changes of the DSRD2 (coupled to the KG filter) output with housing temperature changes were measured first with a black perspex housing and secondly with a white perspex housing but without a filter.

3.3.1. The DSRD2 housing temperature (with a black perspex). Figure 20 is a plot of direct solar radiation measured in volts using the DSRD2 (coupled to the KG filter) and the NIP together with the measurements of the temperature in degrees centigrade inside the housing of the DSRD2.

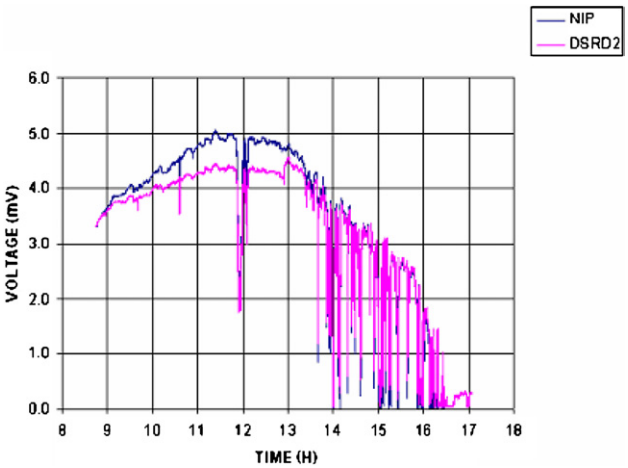

Figure 21. A plot of the direct solar radiation measured in volts using the DSRD2 (with no filter) and the NIP. The black perspex is substituted with a white perspex. The DSRD2 readings are corrected to the NIP readings.

The graph in green describes variations in temperature within the housing. The ambient temperature was not measured as the weather station was not operational at the time of this experiment. However, it is expected that it would be higher because inside the housing there is a shade. The magnitude of the DSRD2 measurements has been corrected to the magnitude of the NIP readings. The plot indicates that around 10:30 the temperature is lowest even though there is an increase of the amount of solar radiation measured by both instruments. At around 16:30 the results show an abrupt decrease in measured solar radiation and this suggests that the sun was obscured. The temperature also falls, but at a slower rate. The temperature rise at around 11:00 with a sudden fall at 12:00 is of significance. If temperature had an effect, the readings by the DSRD2 would have been higher at this period. This is not so. This indicates that the variations of the temperature inside the housing of the DSRD2 do not affect significantly the measurements performed with the DSRD2.

3.3.2. The DSRD2 housing temperature (with a white perspex). Results of the measurements of the direct solar radiation in volts measured using the DSRD2 with the black perspex replaced by a white perspex are presented in figure 21. The DSRD2 in this case is not coupled to any filter, the experiment being purely to test for changes in temperature.

The plot indicates a closeness between the readings of both instruments except in the time interval from 09:00 up to ∼13:30. In this period, the NIP reads higher than the DSRD2. The reason is probably the fact that the sensing element of the DSRD2 is more sensitive to infrared radiation which is predominant when the scattering of the solar beam is intense. The DSRD2, however, still tracks the reference instrument throughout the whole day. This result is not conclusive, however, since a better comparison would have been between the black perspex data and the white perspex data. This was not possible since it would imply the use of another detector whose optical properties may differ from those of the DSRD2 since we would want to take simultaneous measurements.

4. Conclusions

We have developed a silicon diode into a detector for direct solar radiation. The design is very small and versatile for use in rural areas. The detector performs very well with the KG filter. The results are nearly similar to those obtained using an industry designed NIP and so our design is relatively good for use in place of the NIP. This design can be deployed *en masse* to measure and to catalogue the availability of solar radiation particularly in rural areas. The data can be used for the design of solar thermal energy storage (TES) systems [19].

Acknowledgments

This work was carried out at the University of KwaZulu-Natal. We acknowledge the assistance of Mr R van den Heetkamp and of the Norwegian Government under the NUFU renewable energy project. A studentship from the Erduardo Mondlane University is acknowledged by MAM and a studentship from the DAAD by JSPM.

References

[1] Goldening E W 1958 The combination of local sources of energy for isolated communities *Sol. Energy* **2** 7
[2] Reynhart A F A 1959 Mankind, civilization, and prosperity *Sol. Energy* **3** 23
[3] Thekaekara M P 1976 Solar radiation measurement: techniques and instrumentation *Sol. Energy* **18** 309
[4] Jaffe L D 1983 Optimisation of dish solar collectors *J. Energy* **7** 684
[5] Niemann M, Kreuzburg J, Schreitmüller K R and Leppers L 1997 Solar process heat generation using an ETC collector field with external parabolic circle concentrator (PCC) to operate an adsorption refrigeration system *Sol. Energy* **59** 67
[6] Cruz J M S, Hammond G P and Ries A J P S 2002 Thermal performance of a trapezoidal-shaped solar collector/energy store *Appl. Energy* **73** 195
[7] Kalogirou S A 2004 Solar thermal collectors and applications *Prog. Energy Combustion Sci.* **30** 231
[8] Gore B 2003 Scaling up biogas technology in Nepal *Proc. Workshop in energy for development technology (06–08 August 2003, Valley Trust, Durban, South Africa)*
[9] Cuamba B C *et al* 2001 *General characterization of the solar radiation components in Mozambique* unpublished
[10] McDaniels D K 1984 *The Sun Our Future Energy Source* 2nd edn (New York: Wiley)
[11] Duffie J A and Beckman W A 1991 *Solar Engineering of Thermal Processes* 2nd edn (New York: Wiley)
[12] Twidell J and Weir T 1996 *Renewable Energy Resources* 1st edn (Cambridge: Cambridge University Press)
[13] Goswami D Y, Kreith F and Kreider J F 1999 *Principles of Solar Engineering* 2nd edn (Philadelphia: Taylor and Francis)
[14] Burr-Brown 1996 Optical sensors *IC Data Book* (Tucson: PP)
[15] Ryer A 1998 *Light Measurement Handbook* (Newburyport, USA: International Light, Inc.)
[16] Myers D R, Stoffel T L, Reda I, Wilcox S M and Andreas A M 2002 Recent progress in reducing the uncertainty in and improving pyranometer calibrations *J. Sol. Energy Eng.* **124** 44
[17] Ångström A and Rodhe B 1996 'Pyrheliometric measurement with special regard to the circumsolar sky radiation', Newport R.I. and Swedish Meteorological and Hydrological Institute, Tellus XVIII., Trigger
[18] McPherson M 2004 The space charge relaxation behaviour of silicon diodes irradiated with 1 MeV neutrons *Nucl. Instrum. Methods* A **517** 42
[19] Mawire A and McPherson M 2007 Experimental characterisation of thermal energy storage system using temperature and power controlled charging *Renew. Energy* at press doi:10.1016/j.renene.2007.04.021